Hindawi
Geofluids
Volume 2018, Article ID 7596138, 15 pages
https://doi.org/10.1155/2018/7596138

Research Article

Effects of Maceral Compositions of Coal on Methane Adsorption Heat

Yingke Liu,[1,2] Jianhong Kang,[1,2] Fubao Zhou,[1,2] Yanming Fan,[1] and Haijian Li[1]

[1]*Faculty of Safety Engineering, China University of Mining & Technology, Xuzhou, Jiangsu 221116, China*
[2]*Key Laboratory of Gas and Fire Control for Coal Mines (Ministry of Education), China University of Mining & Technology, Xuzhou, Jiangsu 221116, China*

Correspondence should be addressed to Fubao Zhou; zfbcumt@gmail.com

Received 17 October 2017; Revised 6 February 2018; Accepted 30 April 2018; Published 5 June 2018

Academic Editor: Egor Dontsov

The role of maceral compositions (vitrinite and inertinite) in the adsorption characteristics of coal has not been fully understood in terms of energy. In this study, using a microcalorimeter, the adsorption heat of maceral compositions for methane is directly measured for five groups of Chinese coal samples with different coal ranks. The results show that the adsorption heat of the maceral concentrates varies with increasing coal rank, but for the same coal sample, the vitrinite concentrates have a higher adsorption heat than the inertinite concentrates. Furthermore, the adsorption heat of both vitrinite and inertinite concentrates is highest at the long-flame coal stage. This finding indicates that the coalification and maceral compositions have significant effects on the adsorption heat of coal for methane. It is observed that although the inertinite concentrates have a larger pore volume, they are less microporous than their rank equivalent vitrinite concentrates, resulting in lower adsorption heat. Furthermore, it is revealed that the adsorption heat of both vitrinite and inertinite concentrates is primarily correlated to the content of oxygen-containing functional groups and aliphatic hydrocarbons.

1. Introduction

Coalbed methane (CBM, also known as gas in coal mines) is a type of unconventional gas resource but is also a hazardous gas in underground coal mining and a greenhouse gas. CBM has a greenhouse effect that is 20 times that of carbon dioxide. Motivated by the coalbed methane exploitation, as well as the need to improve the environment, gas storage and transport in coal seams have received considerable attention and continue to be an intense research topic [1, 2]. Unlike a conventional gas reservoir, most gas in coal seams is originally adsorbed on the porous coal matrix, rather than being stored as a free gas. The gas adsorption capacity of coal is one critical issue for the estimation of a coalbed methane reservoir, coalbed methane production, and carbon dioxide sequestration with enhanced CBM recovery [3]. As a result, the study of adsorption characteristics of coal has been an ongoing and important research area in this field [4, 5].

Over recent decades, extensive theoretical and experimental research has been performed on gas adsorption by coal, most of which focused on the effects of physical and chemical properties of coal (such as maceral and mineral composition [6], pore structure [7], and functional group content [8]) and experimental conditions (such as temperature [9], pressure [10], adsorbates [11], and moisture [12]). For example, Jian et al. [13] investigated the coal samples at the vitrinite reflectance of 0.24~0.65% using mercury porosimetry and isothermal adsorption. It was observed that the coal rank was not the main factor affecting the adsorption capacity of coal, while the change of the micropore volume had a significant influence on the adsorption capacity. In addition, coal that has a large specific surface area and is rich in aromatic structure has a high adsorption capacity with methane. Wang et al. [14] studied the adsorption isotherms under low temperature conditions. These researchers' results indicated that the low temperature inhibited the migration of methane in coal seams but could improve the adsorption capacity of coal for methane. With a method combining SEM-EDS and infrared thermal imaging, Feng et al. observed the meso structures with different maceral compositions and

the methane distribution and evolution characteristics in coal [15, 16]. Pini et al. [17] conducted theoretical and experimental investigations on the adsorption isotherms for carbon dioxide, methane, and nitrogen and observed that the adsorption capacity of coal decreased with the increase of vitrinite reflectance. Based on an overview of these references, it was observed that the adsorption volume is usually used to describe the adsorption characteristics of coal for methane. However, the experimentally measured adsorption volume is actually the total volume of gas adsorbed into the pore structure, which includes the adsorbed gas, as well as the free gas, while the theoretically calculated adsorption volume largely depends on the choice of adsorption models and corresponding assumptions [17, 18]. It has been reported that the Langmuir model underestimates the sorption capacity in coal by approximately 30% at 15 MPa [19]. As a result, the adsorption volume has certain limitations for characterizing the adsorption capacity of coal for methane.

Conversely, gas adsorption by coal is essentially the interaction between the molecular structure of coal and gas molecules, which is normally an exothermal process. The heat of adsorption is an inherent property of the adsorption process, reflecting the energy state of gas molecules on the surface adsorption field of coal. Thus, adsorption heat can be used to characterize the adsorbent material energetically and is needed to provide basic data for developing new theories of adsorption equilibria and kinetics [20]. In the literature, there have been several studies examining the adsorption heat accompanying adsorption process. Nodzeński [21] calculated the isosteric heats of sorption methane and carbon dioxide on hard coal using the thermal sorption equation of the virial form. Bülow et al. [22] introduced the method for calculating the isosteric adsorption heat using the Clausius-Clapeyron equation. Chikatamarla and Crosdale [23] calculated the isosteric heats of methane on dry Australian coals based on the Langmuir and BET isotherm models. From a modified Dubinin-Radushkevich model, Day et al. [4, 24] estimated the adsorption heat of carbon dioxide on coal under supercritical conditions. In addition, using the molecular simulation method of quantum chemistry, Jiang et al. [25] and Chen et al. [26] calculated the adsorption heat of methane on coal. Tang et al. calculated the heat of adsorption of methane in such geomaterials as coal and shale by considering the contribution of the adsorbed volume and real gas behavior [27, 28]. In conclusion, the adsorption heat in these studies was calculated by modeling the adsorption isotherms on the basis of molecular simulation. However, the accuracy of molecular simulation is significantly influenced by the selection of the chemical structure model of coal and potential function of the force field [29]. In addition, most estimates of the adsorption heat made from adsorption equilibrium data are subject to potential uncertainty due to the widely varying estimates of model parameters [4]. For example, determining the adsorption heat from the BET isotherms has been criticized because this model assumes that the adsorption heat is constant during the monolayer adsorption but drops to zero after the monolayer is completed [24]. The calculation of mixture heats from extension of the Clapeyron equation is impractical [30].

Compared with the calculation method of adsorption heat as mentioned above, the method of calorimetric measurement for determining adsorption heat of coal for methane has received little attention. However, it is very necessary to perform calorimetric adsorption experiments because the calculation method of adsorption heat hardly takes into account the energetic heterogeneity of coal [20]. To date, there have been few studies on this subject. Glass and Larsen [31] directly measured the isosteric heat of adsorption of various sorbates onto coal using an inverse chromatographic method. Taraba [32] measured the adsorption heat of gas onto coal when studying the competitive adsorption of methane and carbon dioxide. More recently, Zhou et al. [33] studied the effects of coal functional groups on the adsorption microheat of coalbed methane using a C80 microcalorimeter.

Despite the significant effects of the coal type on gas adsorption by coal, no agreement has been reached on how the maceral compositions are correlated to the adsorption capacity of coal for methane [34]. Most studies agree that vitrinite-rich coals have a greater methane adsorption capacity than inertinite-rich coals at the same rank [35]. However, others have found poor or no correlation between adsorption capacity and maceral compositions [4, 36, 37]. To better clarify this confusion on the possible correlation between maceral compositions and methane adsorption capacity, in this study, the effects of maceral compositions on the adsorption characteristics of coal for methane are investigated in terms of adsorption heat by use of the calorimetric measurement method. The maceral concentrates with different coal ranks are prepared by the hand picking and density fraction methods and then are characterized by multipoint Brunauer-Emmett-Teller (BET) measurement and Fourier-transform infrared spectroscopy (FTIR spectroscopy). The correlations between the adsorption heat of maceral concentrates and corresponding pore structure and coal functional groups are discussed in detail.

2. Materials and Methods

2.1. Collection of Coal Samples. Six groups of coal samples were collected from Chinese coal mines. The geological information of coal seams from which the samples were collected is shown in Table 1, and the physical parameters of the collected coal samples are listed in Table 2. Coal sample numbers 1 to 5 were used to investigate the effects of maceral compositions of coal on methane adsorption heat, while number 6 sample was used to compare the isosteric heat of adsorption calculated from adsorption isotherms with that obtained from calorimetric heat. According to the National Standard GB/T 5751-2009 [38], the coal ranks of coal sample numbers 1 to 5 are long-flame coal, fat coal, coking coal, lean coal, and anthracite, respectively. Coal samples were hermetically sealed in bags at 5°C.

2.2. Separation and Preparation of Maceral Concentrates. Coal macerals refer to the basic compositions identified by optical microscopy, primarily including organic macerals and inorganic macerals. According to the genetic type,

Table 1: Geological information of coal seams where the samples were collected.

Coal number	Sampling position	Coal field	Geological formation
Number 1	Coal seam numbers 2-3 in Yuejin Coal Mine	Yima	Yima formation of the middle Jurassic system
Number 2	Coal seam number 24 in Shanjiaoshu Coal Mine	Panxian	Longtan formation of the upper Permian system
Number 3	Coal seam number 3 in Renjiazhuang Coal Mine	Ningdong	Shanxi formation of the lower Permian system
Number 4	Coal seam number 9 in Jinjia Coal Mine	Panxian	Longtan formation of the upper Permian system
Number 5	Coal seam number 2 in Baijigou Coal Mine	Helanshan	Yanan formation of lower Jurassic system
Number 6	Coal seam number 3 in Chengzhuang Coal Mine	Qinshui	Shanxi formation of the lower Permian system

Table 2: Physical parameters of the collected coal samples.

Coal number	Mass (kg)	$R_{o,max}$ (%)	Proximate (%)				Coal quality indices			Coal rank
			M_{ad}	A_{ad}	V_{ad}	FC_{ad}	V_{daf} (%)	G (%)	Y (mm)	
Number 1	3.6	0.59	7.82	25.12	27.85	39.21	41.53	27.6	—	Long-flame coal
Number 2	2.9	1.12	1.01	8.3	31.57	59.12	34.81	92.1	29.8	Fat coal
Number 3	3.1	1.46	6.03	9.13	29.58	55.26	34.87	84.47	13.7	Coking coal
Number 4	4.2	2.11	0.91	13.42	8.66	77.01	10.11	3.2	—	Lean coal
Number 5	3.8	2.86	1.27	5.67	8.9	84.16	9.56	—	—	Anthracite
Number 6	3.4	2.37	0.72	13.88	7.54	77.86	8.83	—	—	Anthracite

organic macerals can be further divided into vitrinite, inertinite, and exinite, among which certain physical differences can be observed. The first difference is their densities. In general, the density of inertinite is the largest, while the density of exinite is the smallest. The second difference is their morphology under the microscope. The morphologies of vitrinite, inertinite, and exinite under the immersion reflection microscope are shown in Figure 1. Since the adsorption capacity of vitrinite and inertinite is much greater than that of exinite [35, 36], this paper only focuses on vitrinite and inertinite.

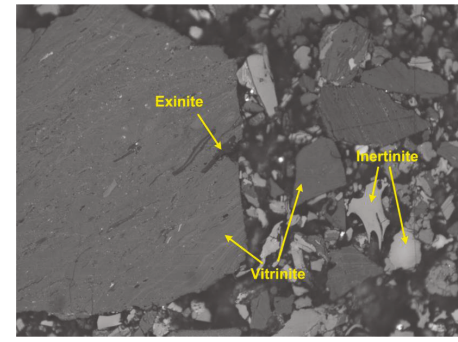

Figure 1: Coal maceral compositions of coal.

2.2.1. Method of Separation and Enrichment. The separation and enrichment methods of coal macerals is based on the physical differences of macerals, such as hand picking and density fractionation. In this study, the hand picking and sieving are used for the preliminary separation of coal macerals, and the method of density fractionation is applied for further enrichment.

(a) Hand picking. Macroscopic compositions of coal refer to the basic unit of coal that can be distinguished by the naked eye, which can be divided into vitrain, clarain, durain, and fusain. The gloss of four macroscopic compositions is gradually weakened. After the coal sample was cracked by a hammer, macroscopic compositions were separated and collected on the basis of the differences of coal color and gloss. In general, vitrain and clarain are rich in vitrinite, while durain and fusain are rich in inertinite.

(b) Sieving. Since the brittleness and the Hardgrove Grindability Index (HGI) of vitrain are lower than those of fusain [39], the vitrinite gathers in large coal particles and can be easily broken into pieces, while the inertinite gathers in small coal particles and can be easily broken into powder. Thus, the larger particle size helps to obtain vitrinite concentrates of higher purity. Otherwise, the particle size should be as small as possible in order to obtain inertinite concentrates of higher purity. Considering that too-small particles will affect the subsequent experiments, a mesh of 60~80 (0.2~0.25 mm) particle size of the coal samples was used in this study.

(c) Density fractionation. The principle of density fractionation is based on the density differences of vitrinite and inertinite. Coal samples of certain particle size were added into the heavy liquid of different densities and were separated by the centrifugal method. The main apparatus for density fractionation consists of an electronic balance, KJLXCD-4004L centrifugal precipitation machine, drying oven, and liquid densimeter. Carbon tetrachloride and benzene were used as the heavy liquid. Finally, the vitrinite and inertinite

concentrates were obtained through the processes of sampling, centrifugation, filtration, and drying.

2.2.2. Method of Detection and Analysis. After the maceral concentrates were prepared by the separation and enrichment as described above, the method of counting pixels was used to quantitatively determine the content of each maceral composition. First, the sample was labeled with a plurality of grids. While moving the microscope lens to the grid nodes, the cross-center of the lens was observed. If the cross-center was located on certain coal particle, this grid was assumed to be an available point. Furthermore, the maceral composition of this coal particle represented the maceral composition of the current grid. According to the National Standard GB/T 8899-2013 [40], more than 500 available points should be recorded in order to accurately measure the content of maceral compositions. The main procedure of this method is described as follows:

(a) Preparing the slice of maceral concentrates: Unsaturated polyester resin, curing agent, and promoter were mixed in the volume ratio of 100 : 4 : 4. Maceral concentrates and binder were mixed in the mass ratio of 10 : 7. The two mixtures were blended and poured into a cold plastic mold.

(b) Polishing the slice: An automatic polishing-grinding machine was used to polish the slice. After being polished, the slice was washed by water and then cleaned by an ultrasonic cleaner.

(c) Counting pixels under a microscope: The polished slice was placed on the microscope stage, and a drop of oil was dripped on the surface of the polished slice such that the slice object was immersed in oil. The focal length was adjusted so that the coal macerals could be clearly observed. After that step, more than 500 available points were measured according to the method of counting pixel, and the data were automatically recorded by a VB computer program.

2.3. Experimental Method

2.3.1. Determination of Adsorption Heat of Coal for Methane. The adsorption heat of methane on maceral concentrates was directly measured using a C80 microcalorimeter produced by Setaram Company in France. The microcalorimeter consists of a host and a gas-circulating pool that has an inlet for gas intake and an outlet for gas discharge. The testing temperature ranges from room temperature to 300°C, and its control accuracy is ±0.001°C with a resolution of 0.1 μw. Furthermore, the gas-circulating pool is surrounded inside by more than 400 pairs of thermocouples to measure the heat flux from the circumferential direction.

The experimental temperature and ambient pressure in both sample and reference vessels were set to 15°C and 0.101 MPa, respectively. The effects of the particle size, quantity of coal samples, and the gas flow rate were taken into account to measure the adsorption heat more accurately.

(a) Size of coal samples: By repeated tests, a particle size of 60~80 mesh was used in this study.

(b) Quantity of coal samples: If the quantity is too small, the gas cannot fully adsorb onto the coal. If the quantity is too large, the programmed sample temperature may deviate from the environmental temperature, resulting in large experimental errors. Considering the capacity of the sample cell and the above factors, 2.5 g of coal samples was used in the current experiment.

(c) Gas flow: To guarantee sufficient methane adsorption, the gas flow was set to 30 mL·min^{-1} in consideration of the experimental accuracy and efficiency.

Furthermore, coal samples may adsorb other gases when they are exposed to air, which affects the accuracy of methane adsorption experiment. Thus, the vacuum-pumping system was used to extract these other gases from the vessels and coal matrix before the test. The vacuum pumping took one hour off after eight hours extracting and this working pattern repeated three times, and, namely, the total time of vacuum pumping was approximately 24 hours. Next, methane was injected into the gas circulating pool.

2.3.2. Determination of Coal Functional Group Types and Contents

(a) Fourier-Transform infrared spectroscopy: The infrared spectroscopy experiments were carried out on a VERTEX 80v Fourier-transform infrared spectrometer which was produced by Bruker Corporation in Germany. The scanned area was 400–4000 cm^{-1} with a resolution of 4 cm^{-1}. To obtain accurate infrared spectrograms, coal samples used in the experiment were smaller than 200 mesh (<76 μm) and were dehydrated for 24 hours. The coal samples were prepared by the KBr disc technique. Pulverized coal was mixed with KBr in the ratio of 1 : 180 (the total weight is 0.1 g). A KBr disc (0.1 g) was used as a blank background.

(b) Types and contents of surface functional groups: The type and content of functional groups on maceral concentrates were obtained by the qualitative and semiquantitative analysis of the infrared spectrograms. First, according to the peaks on the infrared spectrograms, the major functional groups was determined by comparing the attribution of absorption frequency of the coal molecules with the coal molecular structure. The overlapped peaks could be separated by the peak resolution function, such as the OMNIC software. Then, the content of functional groups was analyzed qualitatively by calculating the peak areas for the functional groups. The semiquantitative analysis of the infrared

spectrograms is based on the Lambert-Beer law, which is given as [41]

$$A(\nu) = \lg \frac{1}{T(\nu)} = K(\nu)bc, \quad (1)$$

where $A(\nu)$ is the absorbance, $K(\nu)$ is the absorbance coefficient, b is the thickness of coal sample, c is the concentration of coal sample, and $T(\nu)$ is the percent transmittance.

2.3.3. Aided Tests

(a) Pore characteristics of maceral concentrates: The pore structure of coal samples was characterized by the method of low temperature liquid nitrogen adsorption, which was carried out on a nitrogen adsorption-desorption spectrometer (BET) produced by Japanese BEL Company. The pressure range is 0~133 KPa with a resolution of 1.6×10^{-5} Pa.

(b) Proximate analysis: The proximate analysis including water (M_{ad}), ash (A_{ad}), volatile (V_{ad}), and fixed carbon (FC_{ad}) was carried out on an SDTGA5000 automatic analyzer produced by the Chinese Sande Company. According to the National Standard GB/T 5751-2009 [38], the type of coal can be determined by the dry ash-free basis volatile (V_{daf}), caking index (G), and maximal thickness of the plastic layer (Y).

(c) Mean maximum reflectance of vitrinite: The determination of the mean maximum reflectance of vitrinite ($R_{o,max}$, %) in the coal samples was performed in compliance with the National Standard GB/T 6948-2008 [42] and was recorded by an Axio Imager microscope produced by the Carl Zeiss Foundation Group.

3. Results and Discussion

The adsorption of gas molecules on coal surface is definitely accompanied by the changes of energy. Compared with the adsorption capacity characterized by the adsorption isotherms, the adsorption heat of gas on coal can reflect the adsorption capacity in terms of energy. In this section, based on a comparison between isosteric heat of adsorption calculated from adsorption isotherms and that obtained from calorimetric heat, we mainly focus on how the coalification and maceral compositions of coal affect the adsorption heat of coal for methane.

3.1. Isosteric Heat of Adsorption and Calorimetric Heat of Adsorption of Methane. The isosteric heat of adsorption is defined as the difference of partial molar enthalpy in the gas phase and the excess partial molar enthalpy in the adsorbed phase [43]. The isosteric heat of adsorption can be derived from the Clausius-Clayperon equation as follows [43, 44]:

$$\frac{d \ln P}{dT} = \frac{q_{st}}{RT^2}, \quad (2)$$

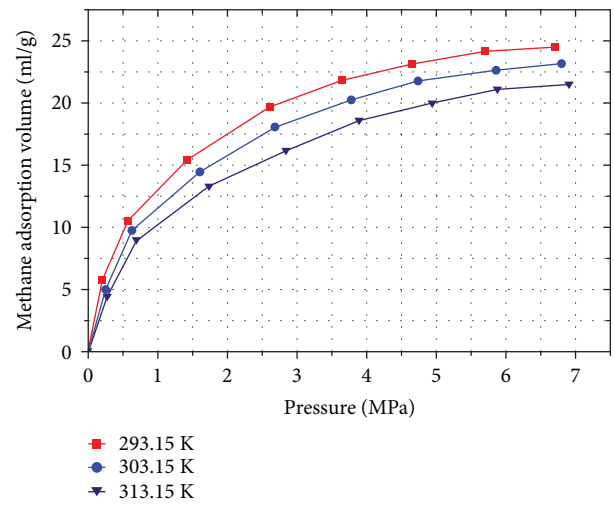

Figure 2: Adsorption isotherms of methane at different temperatures.

where q_{st} is the isosteric heat of adsorption, R is the gas constant, T is the absolute temperature, and P is the pressure.

Integrating both sides of (2), (2) can be expressed as

$$\ln P = \frac{k}{T} + c, \quad (3)$$

where k is the slope of the straight line for ln$P$-1/T, and it can be calculated as follows:

$$k = \frac{-q_{st}}{R}. \quad (4)$$

According to (4), q_{st} can be obtained as follows:

$$q_{st} = -kR. \quad (5)$$

Taking number 6 coal sample as an example (Table 1), the adsorption isotherms for methane at different temperatures are shown in Figure 2. Based on Figure 2, the relationship between pressures (logarithms) and molar adsorption amounts in adsorption process and the corresponding fitting equations of ln$P$-n are shown in Figure 3, where n is the molar adsorption amount, in mmol/g. According to Figure 3 and those fitting equations of ln$P$-n, the relationship between ln$P$ and 1/T under the conditions with different n can be obtained, as shown in Figure 4. The slope of each fitting line of ln$P$-1/T for different molar adsorption amounts and corresponding isosteric heat of adsorption based on (5) are shown in Table 3.

On the other hand, the adsorption heat of coal for methane measured by C80 microcalorimeter is integral adsorption heat. According to the definitions of isosteric heat of adsorption and integral adsorption heat, the relationship of them can be expressed using the following [45]:

$$q_{st} = \frac{dQ}{dn}, \quad (6)$$

where Q is the calorimetric heat of adsorption, in J/g.

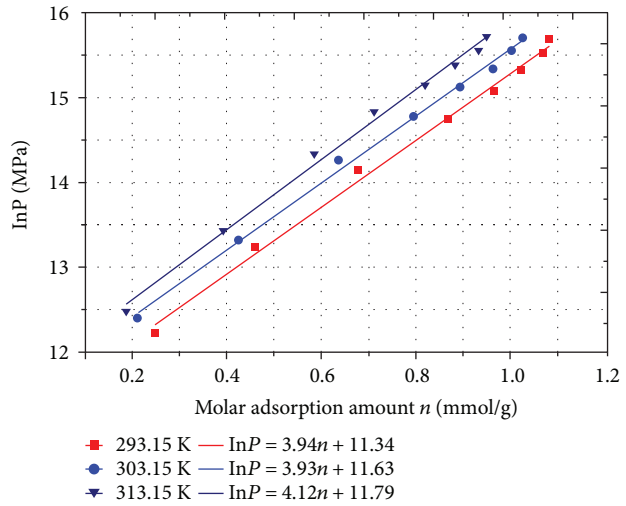

Figure 3: Relationship between pressures (logarithms) and molar adsorption amount.

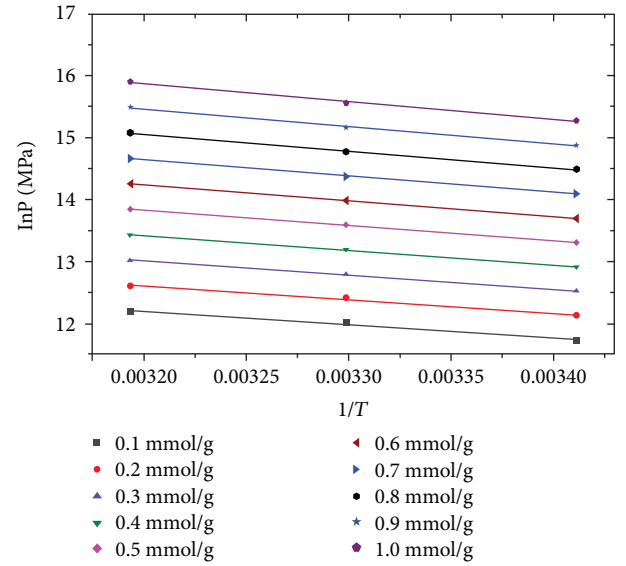

Figure 4: Relationship between ln$P$ and $1/T$ under the conditions with different molar adsorption amount.

According to (6) and the calorimetric heat of adsorption in the adsorption process, the isosteric heat of adsorption can be calculated using the following:

$$q_{st-i} = 0.5 \times \left(\frac{Q_i - Q_{i-1}}{n_i - n_{i-1}} + \frac{Q_{i+1} - Q_i}{n_{i+1} - n_i} \right). \quad (7)$$

For the number 6 coal sample, the calorimetric heat of adsorption for methane measured by C80 microcalorimeter in the adsorption process is shown in Figure 5. According to Figure 5 and (7), the isosteric heat of adsorption obtained from measurement using C80 microcalorimeter is shown in Table 4.

Table 3: Slope of each fitting line of ln$P$-$1/T$ and corresponding isosteric heat of adsorption obtained from adsorption isotherms.

Molar adsorption amount (mmol/g)	Slope	Isosteric heat of adsorption (kJ/mol)
0.1	−2138.6	17.78
0.2	−2221.1	18.47
0.3	−2303.5	19.15
0.4	−2385.9	19.84
0.5	−2468.4	20.52
0.6	−2550.8	21.21
0.7	−2633.3	21.89
0.8	−2715.7	22.58
0.9	−2798.1	23.26
1	−2880.6	23.95

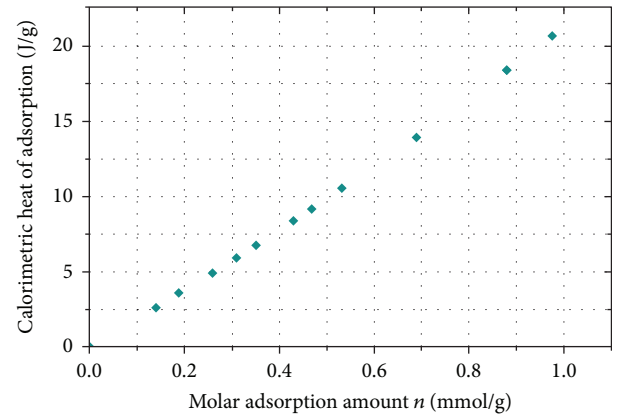

Figure 5: Calorimetric heat of adsorption for methane measured by C80 microcalorimeter.

Table 4: Isosteric heat of adsorption obtained from measurement using C80 microcalorimeter.

Molar adsorption amount (mmol/g)	Isosteric heat of adsorption (kJ/mol)
0.139	19.01
0.188	19.25
0.258	19.66
0.310	19.96
0.350	20.27
0.430	20.72
0.468	21.09
0.532	21.35
0.689	22.46
0.880	23.68

According to Tables 3 and 4, a comparison between isosteric heat of adsorption calculated from adsorption isotherms and that obtained from measurement using C80 microcalorimeter is shown in Figure 6. It is found that there

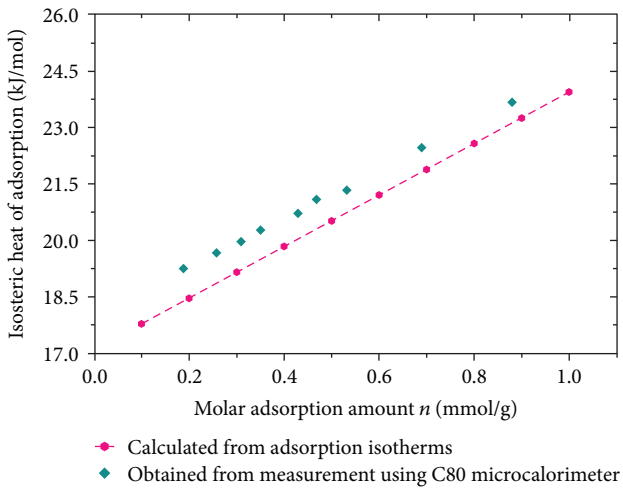

Figure 6: Comparison between isosteric heat of adsorption obtained from adsorption isotherms and that obtained from calorimetric heat.

is just a little difference between them, and they have a same change trend. So the adsorption heat measured using C80 microcalorimeter is reliable and can be used to make more analysis.

3.2. Purity of Maceral Concentrates for Different Coal Ranks. In general, the densities of vitrinite, inertinite, and exinite change with the rank of coal. Even though the degree of metamorphism is the same, the densities of coal samples from different regions may be different from each other. Therefore, when the maceral concentrates were prepared, we needed to determine whether the purity met the experimental requirements. If the experimental requirements are satisfied, the heavy liquid of this density is used for further separation and enrichment. Otherwise, the density of heavy liquid is adjusted, and the following steps are repeated until the desirable purity of maceral concentrates is obtained: separation and enrichment, preparation of powder coal slice, polishing, and microscope observation.

Using the heavy liquid of different density intervals, the purity of vitrinite and inertinite concentrates for five coal samples is shown in Table 5, where VC represents vitrinite concentrates and IC represents inertinite concentrates. For the number 1 coal sample, the VC with a purity of 90% and IC with a purity of 93% were obtained after using two density intervals, respectively. The heavy liquids with three different density intervals were used to concentrate the number 2 coal sample. The purity of number 2 VC in the density interval of 1.26~1.28 g/cm^3 is the highest (86.9%), while the purity of number 2 IC in the density interval of 1.45~1.50 g/cm^3 is the highest (82.4%). For the number 3 coal sample, the purity of VC reached 91.4% in the density interval of 1.28~1.30 g/cm^3, while the highest purity of IC is 87.8% in the density interval of 1.45~1.55 g/cm^3 which is slightly higher than that in the density intervals of 1.40~1.45 g/cm^3 and 1.55~1.65 g/cm^3. For the number 4 coal sample, the VC with a purity of 95.2% was obtained in the density interval of 1.28~1.30 g/cm^3, and the IC with a purity of 97.4% was obtained in the density interval of 1.45~1.55 g/cm^3. Such high-purity samples satisfied the experimental requirements, and no further separation and enrichment continued. For the number 5 coal sample, the purity of VC reached a higher value in both the density intervals of 1.26~1.28 g/cm^3 and 1.28~1.30 g/cm^3. The purity of IC is only 79.3% in the density interval of 1.40~1.45 g/cm^3. After the density of heavy liquid increased to the interval of 1.45~1.50 g/cm^3, its purity increased to 84% accordingly. However, when the density of heavy liquid further increased to the interval of 1.50~1.60 g/cm^3, the purity of IC decreased to 63.6%, and the percentage of minerals increased from 3.2% to 30%. This finding is observed because when the density of heavy liquid is too large, many coal gangue and other minerals are also concentrated in the product.

3.3. Adsorption Heat of Different Maceral Concentrates for Methane. Figure 7 shows the flux of methane adsorption heat released from the VC and IC of different coals. As shown in Figure 7, the heat flux goes up quickly at the beginning of the methane adsorption and later decreases gradually until the equilibrium of adsorption. Additionally, Figure 8 shows the adsorption heat of VC and IC for methane in terms of energy per unit mass of coal. As shown in Figure 8, the adsorption heat of vitrinite concentrate for methane is always greater than that of the inertinite concentrate for all five coal samples, indicating that the adsorption capacity of vitrinite concentrate is larger than that of the inertinite concentrate. This result agrees well with that of Li et al. [46], who observed that the coal surface with a higher content of vitrinite seems to have a faster adsorption rate and higher affinity with methane. This finding also agrees with that of Crosdale et al. [35], who found that in most cases, vitrinite-rich coals have a greater adsorption capacity than their inertinite-rich equivalents. Furthermore, the adsorption heat of maceral concentrates for methane varies with the increasing coal rank. The maximum values of adsorption heat of vitrinite and inertinite concentrates for methane were reached at the long-flame coal stage (number 1 coal sample, $R_{o,max}$ = 0.59%), which were determined to be 6.19 J/g and 4.76 J/g, respectively. The minimum values of 0.19 J/g and 0.05 J/g were reached at the lean-coal stage (number 4 coal sample, $R_{o,max}$ = 2.11%) for the adsorption heat of vitrinite and inertinite concentrates, respectively.

It can also be seen from Figure 8 that in the bituminous coal stage (i.e., 0.59%<$R_{o,max}$ < 2.11%), the adsorption heat of inertinite concentrates for methane decreased monotonically and reached a minimum at the lean-coal stage, while the adsorption heat of vitrinite concentrates for methane fluctuated with the increase of coal rank. In contrast, from the bituminous coal stage to the anthracite stage (i.e., 2.11%<$R_{o,max}$ < 2.86%), the adsorption heat of inertinite concentrates for methane monotonically increased, and the adsorption heat of vitrinite concentrates has a similar trend. Overall, the adsorption heat of maceral concentrates for methane first decreases with the increasing coal rank, reaching the lowest value at the lean-coal stage, and then increases at the anthracite stage. This indicates that the

Table 5: The purity of maceral concentrates by using heavy liquid of different density intervals.

Sample name	Density interval (g/cm^3)	Percentage of macerals			
		Vitrinite (%)	Inertinite (%)	Exinite (%)	Minerals (%)
Number 1 VC	1.26~1.28	89.6	6.6	3.2	0.6
	1.28~1.32	90	4.1	1.7	4.2
Number 1 IC	1.40~1.45	8	87.4	0.7	3.9
	1.45~1.55	2.5	93	0	4.5
Number 2 VC	1.24~1.26	83.1	11.3	4.7	0.9
	1.26~1.28	86.9	8.7	3.5	0.9
	1.28~1.32	81.7	13.3	3	2
Number 2 IC	1.40~1.45	17.6	78	0.6	3.8
	1.45~1.50	13.5	82.4	1.8	2.3
	1.50~1.55	11.4	78.9	2.1	7.6
Number 3 VC	1.26~1.28	87	9.2	3.8	0
	1.28~1.30	91.4	6.7	1.7	0.2
Number 3 IC	1.40~1.45	11.7	86.8	1.6	0.8
	1.45~1.55	8.6	87.8	2.1	1.5
	1.55~1.65	9.3	82.3	1.5	7.9
Number 4 VC	1.28~1.30	95.2	1.4	3.4	0
Number 4 IC	1.40~1.45	7.9	89.5	1.8	0.8
	1.45~1.55	1.3	97.4	0	1.3
Number 5 VC	1.26~1.28	92.3	5.6	2.1	0
	1.28~1.30	94.7	4.5	0.8	0
Number 5 IC	1.40~1.45	18.7	79.3	1.4	0.6
	1.45~1.50	11.2	84	1.6	3.2
	1.50~1.60	5.5	63.6	0.9	30

coalification has significant effects on the adsorption heat of maceral concentrates for methane.

3.4. Correlation between the Adsorption Heat and the Pore Structure of Coal. It is generally understood that high porosity provides great access into the internal microporosity where most of the gas adsorption occurs [4]. Thus, the pore structure of the coal matrix is closely related with the adsorption capacity of coal for methane and is expected to partly account for the variations of the adsorption heat of different maceral concentrates.

The changes of the average pore size and total pore volume are shown in Figure 9. From Figure 9(a), it can be seen that the minimum and maximum average pore sizes of vitrinite and inertinite concentrates for five coal samples are 1.26 nm and 9.69 nm, respectively. According to the pore size classification by Cai et al. [7], pores whose size is less than 10 nm belong to micropores. Therefore, the micropores account for the largest percentage of pore size for the maceral concentrates. In addition, with the increase of $R_{o,max}$, the variations of average pore size for the inertinite concentrates and vitrinite concentrates have the same trends. In contrast, the variation of total pore volume of vitrinite concentrates does not coincide with that of inertinite concentrates, as shown in Figure 9(b). In particular, the total pore volume of inertinite concentrate for the number 1 coal sample reaches 0.0152 mL/g, which is almost 15 times the total pore volume of its rank equivalent vitrinite concentrates.

According to the geological genesis of coal macerals, the vitrinite is mainly formed by the gelatification of wood fiber, while the inertinite is primarily formed by the fusinization of fibrous tissue of plants. The fusinite contains a large number of pores as shown in Figure 10, which explains why the total pore volume and average pore size of inertinite concentrates are greater than those of vitrinite concentrate. As illustrated in Table 5, the purity of inertinite concentrates for five coal sample has little difference, but their pore parameters shown in Figure 9 make a great difference, indicating that although the inertinite concentrates contain abundant fusinite, there are great differences in the pore structure of fusinite for different coal ranks.

An interesting paradox can be found by comparing the results obtained from Figures 8 and 9(b). It has been understood that the larger pore volume corresponds to a stronger adsorption capability of coal for methane [4, 46]. From Figure 9(b), it is clearly observed that the total pore volume of inertinite concentrates is larger than that of vitrinite concentrates, indicating that the inertinite concentrates should adsorb more methane than their rank equivalent vitrinite concentrates. As a result, the adsorption heat of inertinite concentrates for methane should be higher than that of vitrinite concentrates. However, the opposite conclusion is

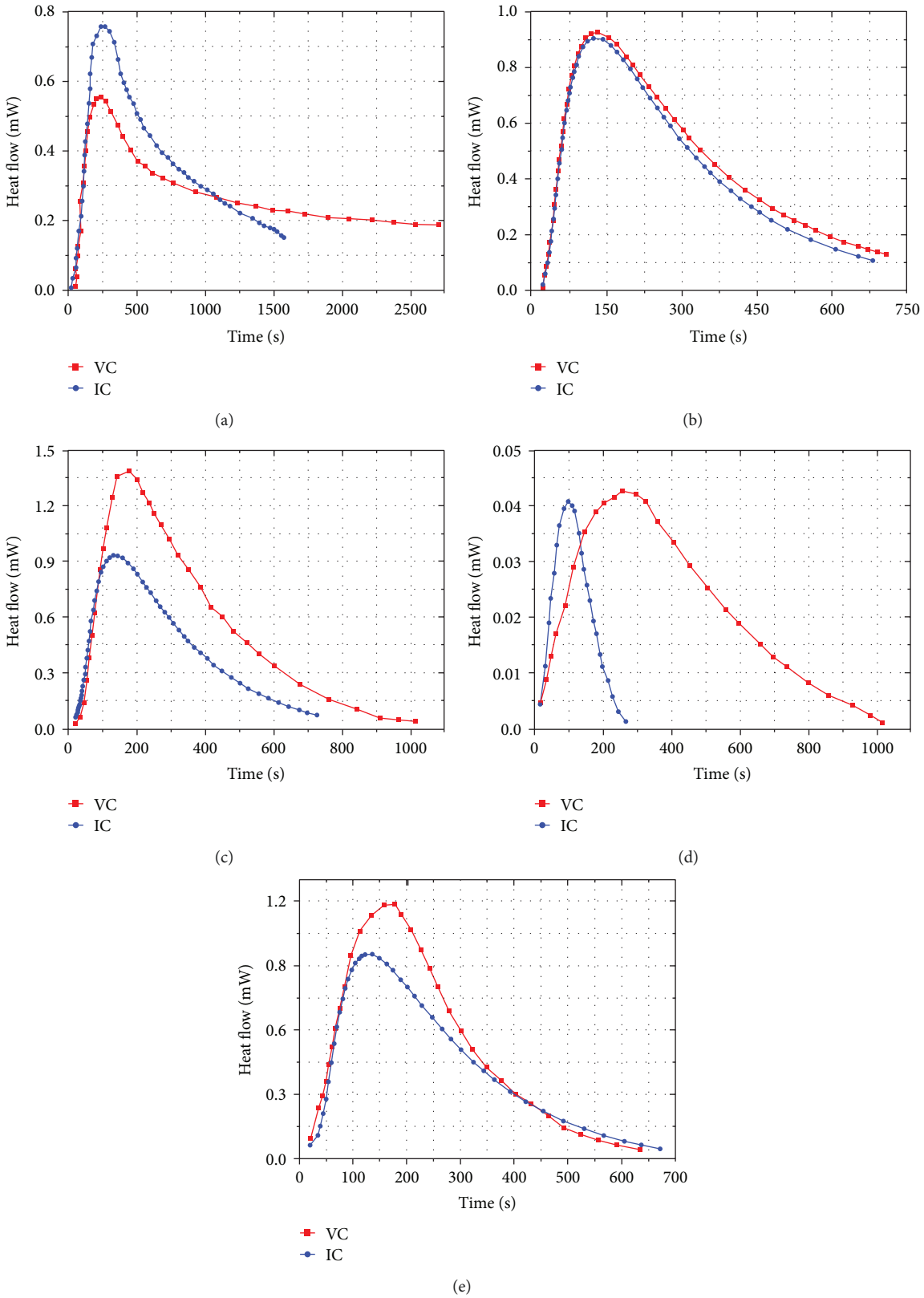

FIGURE 7: Curves of flux of methane adsorption heat released from maceral concentrates of coal sample numbers 1 (a), 2 (b), 3 (c), 4 (d), and 5 (e).

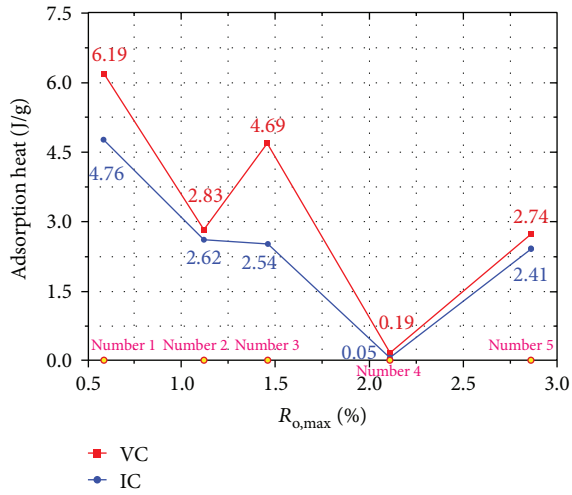

Figure 8: Curves of adsorption heat for maceral concentrates of different coals.

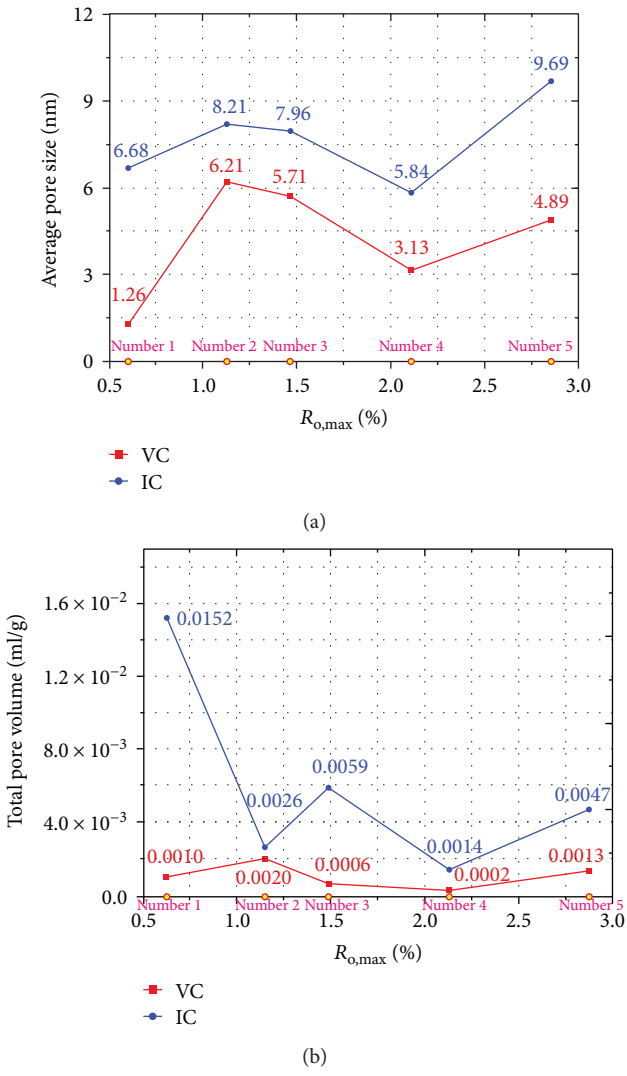

Figure 9: Curves of average pore size (a) and total pore volume (b) for maceral concentrates.

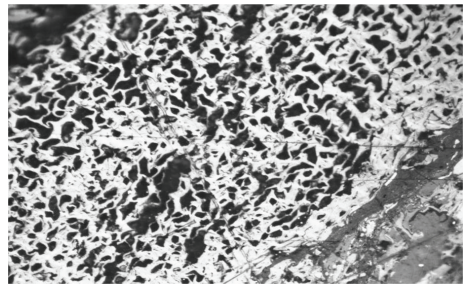

Figure 10: Morphology of fusinite under a microscope.

drawn from Figure 8, where the adsorption heat of the vitrinite concentrates is higher than that of the inertinite concentrates. This abnormal phenomenon may be caused by the following two factors. (1) At low pressures, gas adsorption by coal has traditionally been assumed as a surface monolayer coverage with the Langmuir adsorption model [24, 47]. Although the total pore volume of inertinite concentrates is larger than that of vitrinite concentrates, the inertinite concentrates are more macroporous and less microporous than their rank equivalent vitrinite concentrates, which results in smaller specific surface area and less adsorption heat of inertinite concentrates accordingly. (2) The type and content of surface functional groups of vitrinite and inertinite concentrates are quite different, which could lead to the differences of adsorption heat between vitrinite and inertinite concentrates, as is discussed in the next subsection.

Furthermore, to investigate the correlation between the adsorption heat of maceral concentrates and corresponding pore parameters, the comparison of the maximum heat flow, adsorption heat, and the pore parameters are illustrated in Figure 11. It is shown that with the increase of $R_{o,max}$, the variation of adsorption heat with pore parameters of vitrinite concentrates is notably different from that of inertinite concentrates. For the case of vitrinite concentrates, from the long-flame coal (number 1 coal sample, $R_{o,max} = 0.59\%$) to coking coal stage (number 3 coal sample, $R_{o,max} = 1.46\%$) (i.e., the low- and medium-coal rank), the adsorption heat decreases with the increase of total pore volume and average pore diameter. In other words, the pore parameters are negatively correlated with the adsorption heat. However, from the coking coal (number 3 coal sample) to anthracite stage (number 5 coal sample, $R_{o,max} = 2.86\%$) (i.e., the medium- and high-coal rank), the pore parameters show a positive correlation with the adsorption heat. For the case of inertinite concentrates, the pore parameters are positively correlated with the adsorption heat on the whole.

Additionally, there are regional influences on the porosity of coals [48]. Both coal sample numbers 2 and 4 were collected from Panxian Coal Field, so VC and IC of these two samples have very similar value of the total pore volume (Figure 9), which leads to very small differences between the adsorption heat of vitrinite and inertinite concentrates of sample numbers 2 and 4 (Figure 8). Moreover, the flow rate of methane gas in coal samples is controlled by the porosity of coal, so Figure 11 also shows that with

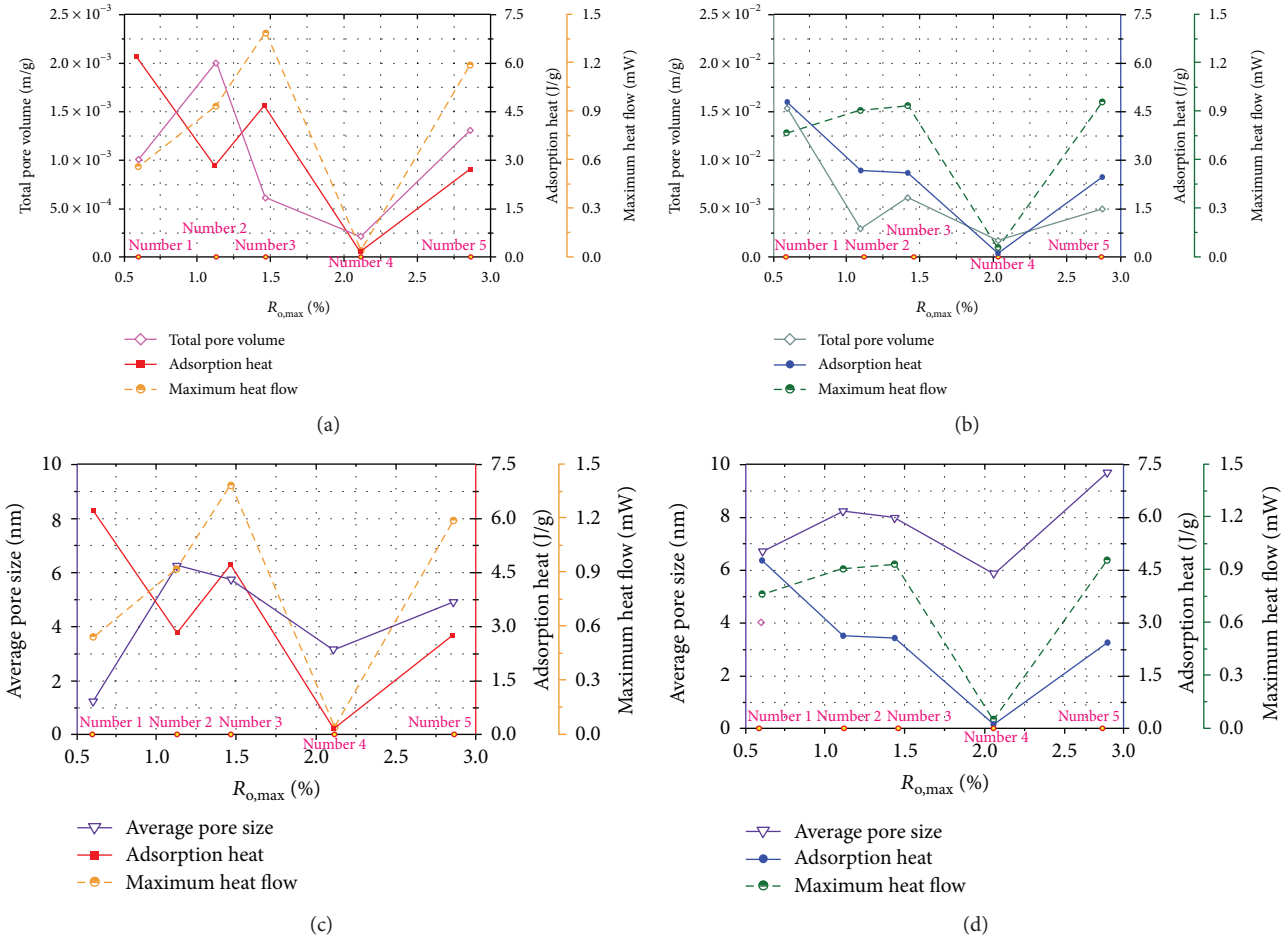

Figure 11: Correlation between the adsorption heat and the total pore volume of VC (a) and IC (b) and the average pore diameter of VC (c) and IC (d), respectively.

the increase of the pore parameters, the maximum heat flow during adsorption goes up.

3.5. Correlation between the Adsorption Heat and the Surface Functional Groups. For a further understanding of the factors influencing methane adsorption and the differences between the adsorption heat of vitrinite and inertinite concentrates, the type and content of chemical functional groups on the surface of maceral concentrates were determined by infrared spectroscopy, which directly affects the adsorption heat of maceral concentrates for methane via the adsorption potential of methane molecules on the coal surface.

Figure 12 shows the peak areas for the surface functional groups together with the adsorption heat of vitrinite and inertinite concentrates. Typical functional groups mainly include the aliphatic hydrocarbons ($-CH_3/-CH_2-/\equiv CH$) and aromatic structures (C=C) and oxygen-containing functional groups (–OH, –COOH–, –COO–, –C–O–, and C=O). The content and distribution of surface functional groups for vitrinite and inertinite concentrates of the same coal sample differ greatly from each other. For the vitrinite concentrates, as shown in Figure 12(a), the oxygen-containing functional groups and aromatic structures dominate the content and distribution of functional groups. With the increase of $R_{o,max}$, the total content of various functional groups in vitrinite concentrates exhibits a downward trend, reaching the minimum value at the lean coal stage (number 4 coal sample, $R_{o,max} = 2.11\%$), and then an upward trend for aromatic structures at the anthracite stage (number 5 coal sample, $R_{o,max} = 2.86\%$). The number 1 coal sample has the highest and balanced distribution of different functional groups. Particularly, the number 4 coal sample has the lowest aliphatic hydrocarbons and aromatic structures, while the number 5 coal sample has the lowest oxygen-containing functional groups. On the other hand, for the inertinite concentrates, as shown in Figure 12(b), the oxygen-containing functional groups are predominant for most coal samples (number 1, number 3, and number 5). The oxygen-containing functional groups in the low-rank coal is the highest (number 1 coal sample, $R_{o,max} = 0.59\%$), but it decreases with the increase of $R_{o,max}$. The content of aliphatic hydrocarbons in the medium-rank coal is the highest (number 2 coal sample, $R_{o,max} = 1.12\%$), but it is lower in the other coal samples. Overall, for five different coal samples, the content of oxygen-containing functional groups in the vitrinite concentrates has few differences from that in the inertinite concentrates, but the content of aliphatic hydrocarbons and aromatic structures in the

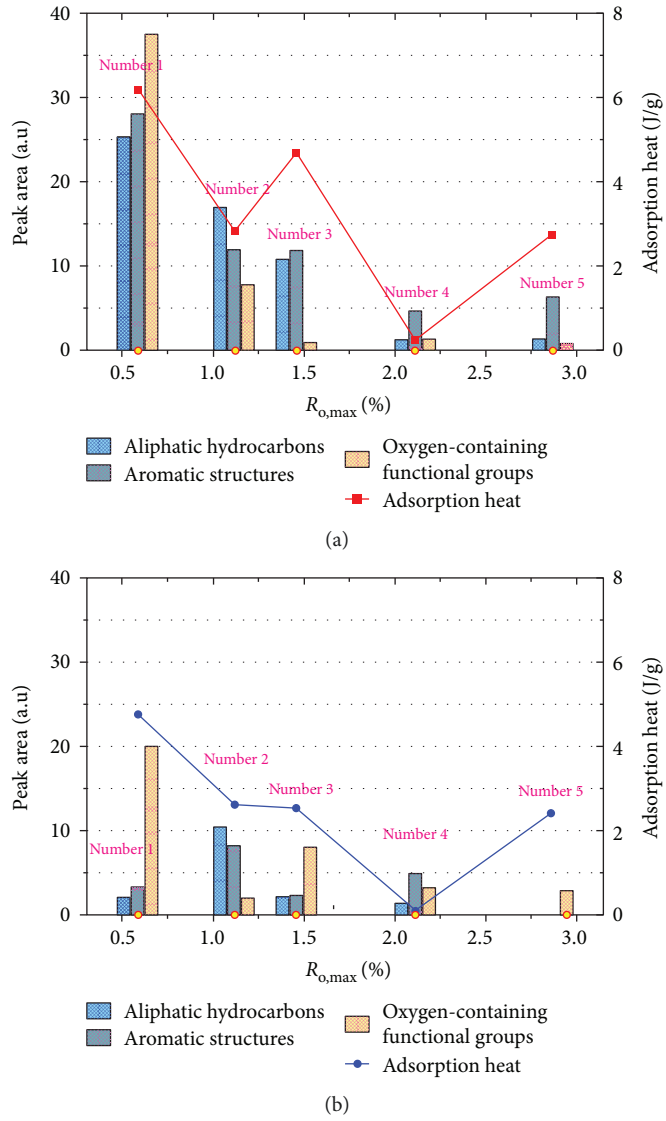

Figure 12: Correlation between the adsorption heat and the surface functional groups of vitrinite (a) and inertinite (b) concentrates.

vitrinite concentrates is significantly higher than that in the inertinite concentrates.

The adsorption of methane by coal is physical absorption and depends on an intermolecular force. Larger intermolecular forces and larger molecular polarity of the functional groups of coal are associated with a greater adsorption potential, stability of adsorption, and adsorption heat [49, 50]. In general, oxygen-containing functional groups influence the adsorption heat via the adsorption potential of methane molecules, and the adsorption heat of oxygen-containing functional groups which have stronger polarity is greater than that of other functional groups [33]. Aromatic nuclei and methane molecules are both nonpolar molecules with polar bonds, so the adsorption heat of aromatic structures is very small. While the aliphatic hydrocarbons are polar molecules, their intermolecular forces associated with methane are larger than those of aromatic nuclei [33]. Accordingly, the adsorption heat of aliphatic hydrocarbons for methane is greater than that of aromatic nuclei. However, if the aromatic condensed nuclei have side chains with other types of functional groups, the adsorption heat of aromatic structures increases accordingly.

The variations of adsorption heat of maceral concentrates for different coal samples are closely related with the type and content of typical functional groups. As shown in Figure 12, it is shown that the variation tendency of adsorption heat of both vitrinite and inertinite concentrates for methane is positively correlated to the content and distribution of oxygen-containing functional groups and aliphatic hydrocarbons. The long-flame coal (number 1 coal sample, $R_{o,max} = 0.59\%$) has the highest content of oxygen-containing functional groups; thus, the value of adsorption heat is maximum. With the increase of $R_{o,max}$, the content of oxygen-containing functional groups and aliphatic hydrocarbons decreases, which results in a decline of adsorption heat of both vitrinite and inertinite concentrates for methane. For the lean coal (number 4 coal sample, $R_{o,max} = 2.11\%$), the adsorption heat is minimum with the lower content of total functional

groups. From the lean-coal stage (number 4 coal sample) to the anthracite stage (number 5 coal sample, $R_{o,max}$ = 2.86%), the adsorption heat of maceral compositions of coal has an obvious increase with few changes of the content of oxygen-containing functional groups and aliphatic hydrocarbons. This is because both the total pore volume and the average pore size increase significantly (Figure 11). Additionally, for the same coal sample, the peak areas of oxygen-containing functional groups and aliphatic hydrocarbons for vitrinite concentrates are larger than those for inertinite concentrates. This result suggests that the contents of oxygen-containing functional groups and aliphatic hydrocarbons in the vitrinites may dominate the adsorption heat of coal for methane.

4. Conclusions

The objective of this study is to investigate the effects of maceral composition of coal on the adsorption heat of methane on coal and further deepen our understanding of the adsorption theory of coalbed methane. To this end, five groups of Chinese coal samples with different coal ranks were collected to prepare the vitrinite and inertinite concentrates. The adsorption heat of maceral concentrates for methane was directly measured by the method of calorimetric measurement. The main findings of this study are summarized as follows.

(1) For all coal samples, the adsorption heat of vitrinite concentrates for methane is higher than their rank equivalent inertinite concentrates. Furthermore, the adsorption heat varies with the increasing coal rank. The highest adsorption heats of vitrinite and inertinite concentrates are achieved at the long-flame coal stage, which are approximately 6.19 J/g and 4.76 J/g, respectively. The lowest adsorption heats of vitrinite and inertinite concentrates are achieved at the lean coal stage, which are 0.19 J/g and 0.05 J/g, respectively.

(2) For the vitrinite concentrates, the total pore volume and average pore size are negatively correlated with the adsorption heat at the low- and medium-coal ranks, but a positive correlation is observed at the medium- and high-coal ranks. For the inertinite concentrates, the total pore volume and average pore size are positively correlated with the adsorption heat as a whole.

(3) The type and content of surface functional groups for vitrinite and inertinite concentrates are quite different. Overall, the adsorption heat of both vitrinite and inertinite concentrates is primarily correlated to the content of oxygen-containing functional groups and aliphatic hydrocarbons.

(4) For the same coal sample, the peak areas of oxygen-containing functional groups and aliphatic hydrocarbons for vitrinite concentrates are larger than those for inertinite concentrates. That is, the fundamental reason of the fact that the adsorption heat of vitrinite concentrates for methane is higher than their rank equivalent inertinite concentrates.

Conflicts of Interest

The authors declare that there are no conflicts of interest regarding the publication of this paper.

Acknowledgments

This work was supported by the National Key R&D Program of China (2016YFC0802900), the National Natural Science Foundation of China (51774277), and the Fundamental Research Funds for the Central Universities (2013QNA02).

References

[1] T. A. Moore, "Coalbed methane: a review," *International Journal of Coal Geology*, vol. 101, pp. 36–81, 2012.

[2] A. Busch and Y. Gensterblum, "CBM and CO2-ECBM related sorption processes in coal: a review," *International Journal of Coal Geology*, vol. 87, no. 2, pp. 49–71, 2011.

[3] C. M. White, D. H. Smith, K. L. Jones et al., "Sequestration of carbon dioxide in coal with enhanced coalbed methane recovery – a review," *Energy & Fuels*, vol. 19, no. 3, pp. 659–724, 2005.

[4] S. Day, G. Duffy, R. Sakurovs, and S. Weir, "Effect of coal properties on CO_2 sorption capacity under supercritical conditions," *International Journal of Greenhouse Gas Control*, vol. 2, no. 3, pp. 342–352, 2008.

[5] J. Kang, F. Zhou, G. Ye, and Y. Liu, "An anomalous subdiffusion model with fractional derivatives for methane desorption in heterogeneous coal matrix," *AIP Advances*, vol. 5, no. 12, article 127119, 2015.

[6] M. J. Kotarba and D. D. Rice, "Composition and origin of coalbed gases in the lower Silesian basin, Southwest Poland," *Applied Geochemistry*, vol. 16, no. 7-8, pp. 895–910, 2001.

[7] Y. Cai, D. Liu, Z. Pan, Y. Yao, J. Li, and Y. Qiu, "Pore structure and its impact on CH_4 adsorption capacity and flow capability of bituminous and subbituminous coals from Northeast China," *Fuel*, vol. 103, pp. 258–268, 2013.

[8] S. Hao, J. Wen, X. Yu, and W. Chu, "Effect of the surface oxygen groups on methane adsorption on coals," *Applied Surface Science*, vol. 264, pp. 433–442, 2013.

[9] G. Yue, Z. Wang, X. Tang, H. Li, and C. Xie, "Physical simulation of temperature influence on methane sorption and kinetics in coal (II): temperature evolvement during methane adsorption in coal measurement and modeling," *Energy & Fuels*, vol. 29, no. 10, pp. 6355–6362, 2015.

[10] H. J. Kim, Y. Shi, J. He, H.-H. Lee, and C.-H. Lee, "Adsorption characteristics of CO_2 and CH_4 on dry and wet coal from subcritical to supercritical conditions," *Chemical Engineering Journal*, vol. 171, no. 1, pp. 45–53, 2011.

[11] J. E. Fitzgerald, Z. Pan, M. Sudibandriyo, R. L. Robinson Jr., K. A. M. Gasem, and S. Reeves, "Adsorption of methane, nitrogen, carbon dioxide and their mixtures on wet Tiffany coal," *Fuel*, vol. 84, no. 18, pp. 2351–2363, 2005.

[12] M. Švabova, Z. Weishauptova, and O. Přibyl, "The effect of moisture on the sorption process of CO_2 on coal," *Fuel*, vol. 92, no. 1, pp. 187–196, 2012.

[13] K. Jian, X. Fu, Y. Ding, H. Wang, and T. Li, "Characteristics of pores and methane adsorption of low-rank coal in China," *Journal of Natural Gas Science and Engineering*, vol. 27, Part 1, pp. 207–218, 2015.

[14] Z. Wang, X. Tang, G. Yue, B. Kang, C. Xie, and X. Li, "Physical simulation of temperature influence on methane sorption and kinetics in coal: benefits of temperature under 273.15 K," *Fuel*, vol. 158, pp. 207–216, 2015.

[15] Z. Feng, T. Cai, D. Zhou, D. Zhao, Y. Zhao, and C. Wang, "Temperature and deformation changes in anthracite coal after methane adsorption," *Fuel*, vol. 192, pp. 27–34, 2017.

[16] D. Zhou, Z. Feng, D. Zhao, Y. Zhao, and T. Cai, "Experimental meso scale study on the distribution and evolution of methane adsorption in coal," *Applied Thermal Engineering*, vol. 112, pp. 942–951, 2017.

[17] R. Pini, S. Ottiger, L. Burlini, G. Storti, and M. Mazzotti, "Sorption of carbon dioxide, methane and nitrogen in dry coals at high pressure and moderate temperature," *International Journal of Greenhouse Gas Control*, vol. 4, no. 1, pp. 90–101, 2010.

[18] S. Harpalani, B. K. Prusty, and P. Dutta, "Methane/CO_2 sorption modeling for coalbed methane production and CO_2 sequestration," *Energy & Fuels*, vol. 20, no. 4, pp. 1591–1599, 2006.

[19] R. Sakurovs, S. Day, S. Weir, and G. Duffy, "Temperature dependence of sorption of gases by coals and charcoals," *International Journal of Coal Geology*, vol. 73, no. 3-4, pp. 250–258, 2008.

[20] W. Zimmermann and J. U. Keller, "A new calorimeter for simultaneous measurement of isotherms and heats of adsorption," *Thermochimica Acta*, vol. 405, no. 1, pp. 31–41, 2003.

[21] A. Nodzeński, "Sorption and desorption of gases (CH_4, CO_2) on hard coal and active carbon at elevated pressures," *Fuel*, vol. 77, no. 11, pp. 1243–1246, 1998.

[22] M. Bülow, D. Shen, and S. Jale, "Measurement of sorption equilibria under isosteric conditions: the principles, advantages and limitations," *Applied Surface Science*, vol. 196, no. 1–4, pp. 157–172, 2002.

[23] L. Chikatamarla and P. J. Crosdale, "Heat of methane adsorption of coal: implications for pore structure development," in *Proceedings of the International Coalbed Methane Symposium*, pp. 151–162, Tuscaloosa, AL,USA, 2001, University of Alabama.

[24] S. Day, R. Sakurovs, and S. Weir, "Supercritical gas sorption on moist coals," *International Journal of Coal Geology*, vol. 74, no. 3-4, pp. 203–214, 2008.

[25] W. Jiang, Y. Cui, Q. Zhang, L. Zhong, and Y. Li, "The quantum chemical study on different rank coals surface interacting with methane," *Journal of China Coal Society*, vol. 32, no. 3, pp. 292–295, 2007.

[26] C. G. Chen, X. W. Wei, and X. F. Xian, "AB intio study on the interaction between CH_4 and the coal surface," *Journal of Chongqing University*, vol. 23, no. 3, pp. 77–82, 2000.

[27] X. Tang, Z. Wang, N. Ripepi, B. Kang, and G. Yue, "Adsorption affinity of different types of coal: mean isosteric heat of adsorption," *Energy & Fuels*, vol. 29, no. 6, pp. 3609–3615, 2015.

[28] X. Tang, N. Ripepi, N. P. Stadie, and L. Yu, "Thermodynamic analysis of high pressure methane adsorption in Longmaxi shale," *Fuel*, vol. 193, pp. 411–418, 2017.

[29] H. Hu, X. Li, Z. Fang, N. Wei, and Q. Li, "Small-molecule gas sorption and diffusion in coal: molecular simulation," *Energy*, vol. 35, no. 7, pp. 2939–2944, 2010.

[30] F. Siperstein, R. J. Gorte, and A. L. Myers, "A new calorimeter for simultaneous measurements of loading and heats of adsorption from gaseous mixtures," *Langmuir*, vol. 15, no. 4, pp. 1570–1576, 1999.

[31] A. S. Glass and J. W. Larsen, "Coal surface properties. Specific and nonspecific interactions for polar molecules and surface tensions for hydrocarbons at the surface of Illinois no. 6 coal," *Energy & Fuels*, vol. 8, no. 3, pp. 629–636, 1994.

[32] B. Taraba, "Flow calorimetric insight to competitive sorption of carbon dioxide and methane on coal," *Thermochimica Acta*, vol. 523, no. 1-2, pp. 250–252, 2011.

[33] F. Zhou, S. Liu, Y. Pang, J. Li, and H. Xin, "Effects of coal functional groups on adsorption microheat of coal bed methane," *Energy & Fuels*, vol. 29, no. 3, pp. 1550–1557, 2015.

[34] G. R. L. Chalmers and R. Marc Bustin, "On the effects of petrographic composition on coalbed methane sorption," *International Journal of Coal Geology*, vol. 69, no. 4, pp. 288–304, 2007.

[35] P. J. Crosdale, B. B. Beamish, and M. Valix, "Coalbed methane sorption related to coal composition," *International Journal of Coal Geology*, vol. 35, no. 1–4, pp. 147–158, 1998.

[36] I. Ettinger, I. Eremin, B. Zimakov, and M. Yanovskaya, "Natural factors influencing coal sorption properties: I. Petrography and the sorption properties of coals," *Fuel*, vol. 45, pp. 267–275, 1966.

[37] M. M. Faiz, N. I. Aziz, A. C. Hutton, and B. G. Jones, "Porosity and gas sorption capacity of some eastern Australian coals in relation to coal rank and composition," in *Coalbed Methane Symposium*, pp. 19–21, Townsville, QLD, Australia, 1992.

[38] The National Standards Compilation Group of Peoples Republic of China, *GB/T 5751–2009 Chinese Classification of Coals*, Standards Press of China, Beijing, China, 2009.

[39] A. S. Trimble and J. C. Hower, "Studies of the relationship between coal petrology and grinding properties," *International Journal of Coal Geology*, vol. 54, no. 3-4, pp. 253–260, 2003.

[40] The National Standards Compilation Group of Peoples Republic of China, *GB/T 8899-2013 Determination of Maceral Composition and Minerals in Coal*, Standards Press of China, Beijing, China, 2013.

[41] S. Ye, C. Liu, S. Chen, F. Wang, Y. Jia, and Z. Li, "A judgement method of matrix resin based on infrared spectra of low emissivity coatings," *Infrared Technology*, vol. 38, no. 6, pp. 524–528, 2016.

[42] The National Standards Compilation Group of Peoples Republic of China, *GB/T 6948-2008 Method of Determining Microscopically the Reflectance of Vitrinite in Coal*, Standards Press of China, Beijing, China, 2008.

[43] A. J. Ramirez-Pastor and F. Bulnes, "Differential heat of adsorption in the presence of an order–disorder phase transition," *Physica A: Statistical Mechanics and Its Applications*, vol. 283, no. 1-2, pp. 198–203, 2000.

[44] S. Chattaraj, D. Mohanty, T. Kumar, and G. Halder, "Thermodynamics, kinetics and modeling of sorption behaviour of coalbed methane – a review," *Journal of Unconventional Oil and Gas Resources*, vol. 16, pp. 14–33, 2016.

[45] A. Auroux, *Calorimetry and Thermal Methods in Catalysis*, Springer-Verlag, Berlin, Heidelberg, 2013.

[46] Q. Li, B. Lin, K. Wang, M. Zhao, and M. Ruan, "Surface properties of pulverized coal and its effects on coal mine methane adsorption behaviors under ambient conditions," *Powder Technology*, vol. 270, Part A, pp. 278–286, 2015.

[47] G. F. Cerofolini and L. Meda, "Clustering and melting in multilayer equilibrium adsorption," *Journal of Colloid and Interface Science*, vol. 202, no. 1, pp. 104–123, 1998.

[48] R. Sakurovs, L. Koval, M. Grigore, A. Sokolova, L. F. ruppert, and Y. B. Melnichenko, "Nanometre-sized pores in coal: variations between coal basins and coal origin," *International Journal of Coal Geology*, vol. 186, pp. 126–134, 2018.

[49] J. N. Israelachvili, *Intermolecular and Surface Forces*, Academic Press, Pittsburgh, USA, 2011.

[50] A. Stone, *The Theory of Intermolecular Forces*, Oxford University Press, New York, NY, USA, 2013.